Reinforcing Silicone with Hemp Fiber for Additive Manufacturing

Pantea Koushki[a], Tsz-Ho Kwok[a,*], Lucas Hof[b], Rolf Wuthrich[a]

[a]*Department of Mechanical, Industrial and Aerospace Engineering, Concordia University Montreal, Canada.*
[b]*Department of Mechanical Engineering, Ecole de technologie superieure (ETS), Montreal, QC H3C 1K3.*

Abstract

This study explores the 3D printability of a new material based on silicone and hemp fibers from renewable, sustainable and non-petroleum resources with the aim of enhancing mechanical properties of silicone. Incorporation of fibers improved the mechanical properties of the silicone matrix, but it also adversely affected the printability of silicone due to the high viscosity. Therefore, an additional solvent is added into the composition to alter the viscosity. To mature the composite printing technology, this research aims to find out the desired mixing composition of silicone, hemp fiber, and solvent. The behavior of the new engineered material was analyzed using rheological study to obtain a printable material. The composition containing 15wt% hemp fibers and 20wt% solvent with enhanced mechanical properties displayed the desirable printability. Moreover, the mechanical properties of the 3D printed and molded samples were studied. The results revealed that 3D printed samples outperformed the molded counterparts. Finally, a honeycomb structure and a simple gripper were fabricated to demonstrate the application of the developed material.

Keywords: 3D Printing, Silicone, Hemp fibers, Composites, Elastomer.

1. Introduction

Additive manufacturing (AM) or three-dimensional (3D) printing has been established and implemented in different fields like aerospace and healthcare. It can fabricate a structure with complex geometries directly from a computer-aided design (CAD) model. AM offers advantages over conventional molding methods like the ability to create complex interior structures and different degrees of hardness, which makes it attractive to be applied in different applications. To fabricate functional parts with AM, there is an increasing interest in developing 3D printable polymer composites. Different studies [1] have been done to develop new materials that are compatible with available printers. For instance, polylactic acid (PLA)-wood composite is known as a commercial product, and it has been applied in additive manufacturing of wood products. The most common method for 3D printing this wood-thermoplastics composites is the fused deposition modeling (FDM) [2]. FDM is an extrusion-based process that melts and extrudes continuous filament of thermoplastic materials. It can be used to fabricate composites when the filament is pre-mixed with fibers [3], so the polymer is the base material (matrix).

Although there are some printable thermoplastic composites, few studies focus on the development of elastomer composites. Soft materials are important in various fields like soft robotics and biomedical engineering (implants, prosthetics, and anatomical models). For example, 3D printing of silicone rubber is developed using the direct ink writing (DIW) method. In the DIW process, elastomeric ink is extruded out of 3D printer's nozzle and deposited into pattern when the nozzle moves [4].

Moreover, Joshua et al. [5] employed Stereolithography (SLA)-based 3D printing method which is named 3D magnetic printing to design dense ceramic/polymer composites. Electrically assisted nanocomposite 3D printing was employed by Yang et al. [6] to fabricate artificial meniscus. Silicone is a polymer with an inorganic backbone of Si-O, which is made up of repeating units of siloxane. This inorganic backbone attached to the organics group like alkyl (methyl, ethyl) or phenyl group. Depending on their degree of polymerization and the complexity of the organic groups, silicones can be in the form of oils, greases, rubbers, adhesives, and gel. All forms of silicone have their own usages, and they have applications in medical technology, industrial and manufacturing areas. Silicone's significant characteristics make it suitable to be applied in different fields. For instance, its thermal and chemical resistivity makes it appropriate to be used as an insulator in the electrical field; its hydrophobicity has led to its application in the aerospace field; and its inertness and biocompatibility improve its use as a biomaterial in the biomedical field [7]. However, the main problem of pure silicone rubber is its poor tracking and erosion resistance. Therefore, there is a need to enhance the properties of silicone rubber such that its service life and service efficiency are improved. A cost-effective solution to that is adding fillers to reinforce the silicone [8].

Using glass or carbon fibers as a reinforcement is a common method to improve the mechanical properties of a polymer matrix. However, glass or carbon fibers are not cheap and not environmental friendly. In the exhausting of natural resources, developing new products from renewable and sustainable materials has been attracting increasing attention over the past few years. Naturally grown fibers like hemp, flax or jute are more of interest, particularly as a replacement of inor-

ganic fibers. These natural fibers are cheap, have better stiffness per unit weight and have a lower impact on the environment [9]. Among different natural fibers, hemp fiber has been commonly known as an excellent reinforcement due to its low cost, high strength, and ease of processing and recycling [10]. Although natural fibers provide many advantages over glass fiber, they have some disadvantages [11]. For example, due to the low thermal resistance of natural fibers, some processing techniques like molding and extrusion through a hot nozzle have a strong impact on the fiber cell walls. That is why thermoset resin, which cures in room temperature, was commonly used as a binder in the production of natural fibers composites [12, 13]. Moreover, high moisture absorption is a major disadvantage of natural fibers. The water content decreases the compatibility between the fibers and the non-polar elastomeric matrix, leading to the poor fiber-matrix adhesion and thus low mechanical properties. Therefore, many studies have been done on modifying fiber surface to enhance interfacial adhesion between filler particles and polymer macromolecules as well as their dispersion in the polymer matrix [14, 15]. Different chemical and physical fibers surface treatment have also been used to improve fiber/matrix interfacial adhesion [16]. The desired mixing composition also needs to be found in order to improve the fabrication of composites [17]. However, there is no existing study on how the treatments and fiber-matrix compositions affect the 3D-printability of the composites.

Motivated by the need of 3D-printable functional elastomeric composites, this paper focuses on the study of incorporating hemp fibers into silicone – hemp-fiber reinforced silicone (HFRS), to synthesize an eco-friendly and high-performance 3D printing material. However, the integration of hemp fibers makes the material very viscous and thus causes major difficulties in 3D printing. This work investigates the possibility to increase the printability of HFRS by modifying the material viscosity with the addition of a solvent. The main objective is to determine the impact of hemp fibers and solvent incorporation on tensile strength, force resistance, and 3D printability behavior of HFRS. Rheological tests and physical validations are also performed to determine and validate the desirable weight percents of solvent and hemp fibers in the silicone composition.

2. Methodology

Hemp fibers and silicone were mixed in a form of paste, and the composition was fabricated by an DIW 3D printing process. Hemp fibers from low-cost and sustainable sources were chosen as the reinforcement of the composite. Silicone was selected as the binder material. The main focus of this study is to determine the desirable composition of HFRS to provide enhanced mechanical properties while maintaining the 3D-printability. Therefore, tensile tests were performed on different samples to evaluate the effect of fiber loading and surface treatment on the tensile strength and stiffness of the silicone. The goal is to provide a novel low-cost silicone-based material with enhanced mechanical properties for a wide variety of applications. The major challenge of fabricating HFRS with DIW 3D printing method was that the incorporation of fibers changed the
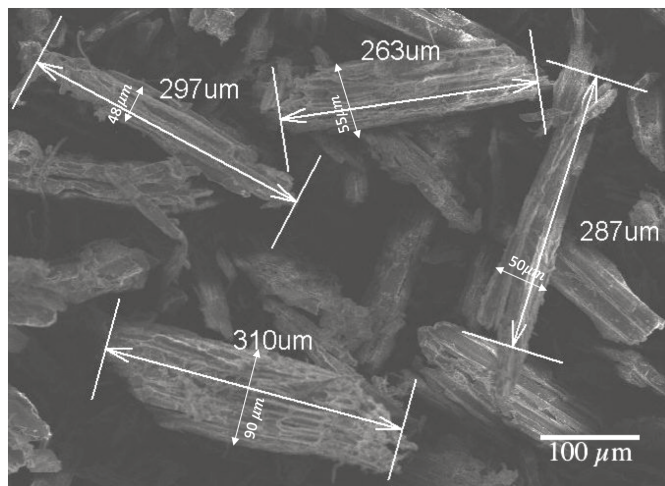

Figure 1: SEM micrographs of hemp fibers.

viscosity and the curing time of silicone, making the silicone unprintable. To solve this problem, a solvent – mineral spirit – is added into the mixture to control the viscosity. The printability of the HFRS composites with different solvent concentrations was evaluated by rheological evaluation and physical validation. In addition, the mechanical properties of 3D printed composites were compared to their molded counterparts, with the same composition, to determine the impact of 3D printing on tensile strength and stiffness of HFRS.

2.1. Materials

All of the materials employed in this work were obtained from commercial sources. Untreated hemp fibers were provided by Ontario Hemp Materials company [18]. The length of the fibers was ranging from 0.2 to 0.4*mm* and the diameter was ranging from 0.04 to 0.09*mm* (see Fig. 1). GE 100% silicone was used in this study. The material 3-Aminopropyltriethoxysilane (3-APS) used for silane treatment was purchased from Gelest Inc. The mineral spirit used as the solvent is a paint thinner produced by Varso.

2.2. Hemp fibers surface modification

Many efforts have been done to modify the surface of natural fibers such that the interfacial adhesion between fibers and matrix is improved. Different physical and chemical treatments for natural fibers including plasma treatment, heat treatment, coupling agents (silane treatment), and mercerization are discussed in the literature [19]. The two most common methods used in the fabrication of natural-fibers-reinforced elastomers are alkali treatment and silane treatment, where the former improves the mechanical adhesion and the latter introduces the chemical bonding.

2.2.1. Alkali treatment

Alkali treatment has been used either alone or as a pretreatment followed by other treatments. Modifying natural fiber's surface with aqueous sodium hydroxide (NaOH) lead to ionization of the hydroxyl group to the alkoxides. It removes a

2

certain amount of lignin and pectin and improves the interaction between the fibers and the polymer matrix by facilitating the exposure of reactive OH groups on the fiber surface. Moreover, mercerization increases the amount of cellulose exposed on the fiber by increasing the number of reaction sites. In other words, NaOH treatment provides rougher surfaces by removing impurities and noncellulosic parts, which increase the adhesive nature of natural fibers. Therefore, this method affects the cellulosic fibril, degree of crystallinity, and extraction of lignin and hemicellulosic compounds [20].

In this treatment, hemp fibers were soaked in a 5% (w/v) NaOH solution for 2 hrs at room temperature. Fibers were further rinsed with distilled water containing acetic acid. This procedure was done a few times until the pH of the rinse water reached 7, and the water no longer indicates any alkalinity. Then the fibers were air dried for two days. At the end, fibers were dried in an oven at 80 °C for 6 hrs.

2.2.2. Silane treatment

Silane coupling agents are widely used due to their wide availability. Silane has alkoxysilane groups at one end that hydrolyze in water and produce silanol, which can react with *OH*-rich surface. Silane as a coupling agent improves the degree of cross-linking in the interface region and increase fiber's surface area for the optimization of fiber resin reinforcement [21, 22, 23]. In other words, alkali treatment leads to a better interaction between the hydroxyl groups in cellulose and the silane coupling agents that can result in chemical bonding with the fiber surface.

Following previous studies [24, 25], silane solution was made by hydrolyzing 5% (wt) silane 3-APS (weight percentage regarding the fiber) in a mixture of water and methanol (40:60 w/w). The pH of the solution was adjusted to 4 with acetic acid. The fibers were immersed in this solution for 3 hrs. Then, they were washed and air-dried for two days, and further dried in an oven at 80 °C for 12 hrs.

2.3. Composite manufacture

Modified fibers were distributed in the silicone matrix using a vacuum mixer ARV-200. The fibers were dispersed in the matrix by mechanical stirring for 2 mins. In this study, two methods were used to fabricate the composite: molding and 3D printing. The molded samples are used to quickly find out the desired composition of fiber and matrix, and are compared with the 3D printed samples.

2.3.1. Molded composites

To determine the desirable composition of hemp fiber and silicone that gives enhanced mechanical properties, dog-bone shape samples with different compositions were molded. The mold, which was used to produce the samples, was made from acrylonitrile butadiene styrene (ABS) material. It is fabricated by 3D printing according to the ASTM D412-16 standard, which is the test method for determining the tensile strength properties of vulcanized thermoset rubber and thermoplastic elastomers. The HFRS samples were prepared in 10 wt%, 15

Table 1: 3D printing parameters for fabricating silicone and HFRS composite.

Material	Layer height (mm)	Infill ratio (%)	Feed rate (mm/s)	Travel speed (mm/s)	Nozzle size (mm)
Silicone	0.3	100%	10	120	0.84
HFRS	0.5	100%	8	120	1.54

wt%, and 20 wt% of hemp fibers, and the composites were obtained with raw fibers, alkali-treated fibers, and alkali&silane-treated fibers. The silcone were cured by the exposure to atmospheric moisture at room temperature for 15 hrs to form cross-linked molecular bonds. Incorporating fibers would increase the viscosity and decrease the curing time. When 15% fibers are incorporated, the curing time was decreased to 7 hrs.

2.3.2. Additive-manufactured composites

After determining the desired composition, the printability of the HFRS composites was evaluated. For 3D printing HFRS, a DIW setup was used, in which the Discov3ry paste extruder [26] was employed. This extruder can be easily added to any existing 3D printer. The Ultimaker line is our printer of choice as it is open-source, well-engineered, and reliable [27]. HFRS composite was loaded into a syringe cartridge, and the Discov3ry extruder system pushed the paste through a feed tube. The material was injected through a nozzle and deposited on platform layer by layer. We employed the optimized 3D printing parameters used in the previous works [28] to fabricate silicone as shown in the Table 1. We further optimized the parameters for printing HFRS by experiments printing the dog-bone shape samples and evaluating their quality. The setting is basically the same, but a larger nozzle diameter is used since the addition of fibers occasionally cause an obstruction in the small nozzle. With respect to that, the layer height is set higher and the print speed is set lower. There is a balance between the printing speed and consistency of feeding. Therefore, $8mm/s$ was chosen as the printing speed to fabricate HFRS, and the printed lines are $1.55mm$ in diameter. This speed was chosen based on experiments, which provides a consistent flow for the whole 3D printing process. This study investigated the effect of different amounts of solvent on 3D printing of HFRS composites.

3. Characterization

3.1. Fourier transform infrared spectrometry (FT-IR)

Fourier transform infrared spectrometry (FT-IR) is an analytical method for investigating the structural identification or confirmation of identified or unidentified product. An infrared spectrum allows to easily discover the presence of significant functional groups. FT-IR study of the untreated, NaOH-treated, and silane-treated hemp fibers were done by using a FT-IR machine (Nicolet 6700 / Smart iTR) to determine the changes in functional groups on the fiber surface. Following the literature [21], all the spectra are recorded in a range of $4000cm^{-1}$ to $500cm^{-1}$, where the expected picks of functional groups are supposed to be presented.
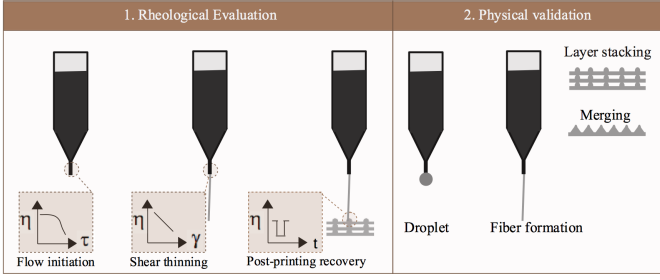
Figure 2: Schematic of the proposed research method to determine the printability of the developed material.

3.2. Scanning electron microscopy (SEM)

To analyze the fracture surface of HFRS composite and to visualize the effect of alkali and silane treatment, scanning electron microscopy (SEM, Hitachi, S-3400N) was utilized. The voids, microstructures, and interfacial interaction of fiber and matrix were determined using SEM at voltage 5 kV, pressure 50 Pa, and at a focusing distance of 5 to 10 mm, for magnification of up to 1000X used in this study. In order to establish effective conductivity for examination, the fracture surfaces of tensile samples were gold sputtered by the Q150T Plus coater produced by Quorum Technologies Ltd, United Kingdom. The coating thickness was about 30 microns.

3.3. Mechanical test

To determine the tensile properties of the products, a tensile test was performed using tensile test machine from Hoskin Scientific company equipped with a 5 kN load cell. The test was developed according to requirements of ASTM D412-06a which is the standard test methods for vulcanized rubber and elastomers-tension. The testing process was carried out at a crosshead speed of 150 mm/min with a gauge length of 40 mm, and the average values of tensile strength and modulus were recorded for all experimental samples of untreated, NaOH-treated, and NaOH/silane-treated HFRS composites.

3.4. Printability assessment

One of the goals in this study is to determine whether HFRS can be fabricated using 3D extrusion printing. The flow continuity during extrusion and the ability to keep its shape after extrusion are the two essential requirements of the material to be 3D-printable. Silicone is proven a printable material. However, the incorporation of hemp fibers increased its viscosity making it unprintable. We proposed to add a solvent into the solution to alter its viscosity. The solvent is a mineral spirit and it will be evaporated after printing. Therefore, we need to find an appropriate solvent concentration that provides 3D printability without changing much the material characteristics. This work used a rheological evaluation and a physical validation to characterize the material printability (see Figure 2).

3.4.1. Rheological evaluations

Rheological studies were executed to measure yield stress, viscosity, and recovery behavior of HFRS composites with different solvent concentrations. These rheological tests describe the properties of the inks before, during and after being extruded in the printing process. To simulate the condition inside the nozzle, it is required to estimate the shear rate inside the nozzle. The shear rate for shear thinning material was calculated via the following equation [29, 30]:

$$\dot{\gamma} = \frac{3n+1}{4n} \frac{32\dot{Q}}{\pi D^3} \tag{1}$$

where D is the nozzle diameter, $\dot{Q}$ is the flow rate, and n is the coefficient derived from the Power Law equation [31]:

$$\sigma = k\dot{\gamma}^n \tag{2}$$

The behavior of each sample can be characterized by fitting the Power Law equation to the shear stress-shear rate rheology plot for each material.

A MCR301 rheometer (Anton Paar) was employed to measure the rheological properties of different samples. A $25mm$ parallel plate with a measurement gap of $1mm$ was used. The samples tested are pure silicone, pure HFRS (i.e., no solvent), and HFRSs with 20 wt%, 30 wt% and 40 wt% solvent. Following the literature and customizing based on our need, the following three rheological experiments at room temperature were carried out:

1. To determine the yield point at which the material first started to flow, a shear stress ramp ranging from 0.01 to $100Pa$ was applied for all samples.
2. To investigate the shear thinning properties of the samples, rotational shear viscosity measurements were done in flow mode in a range of $[\dot{\gamma}_{min} \ \dot{\gamma}]$.
3. To determine the materials recovery behavior after exposure to shear rates, the rotational recovery behavior were performed by simulating before, during, and after extrusion, i.e., first, a low shear rate ($\dot{\gamma}_{min}$) for $200s$; second, a high shear rate ($\dot{\gamma}$) for $100s$; and third, a low shear rate $\dot{\gamma}_{min}$ again for $200s$.

The low shear rate is set to a very small value to simulate the situation at rest (i.e., $\dot{\gamma}_{min} = 0.01 s^{-1}$) and the shear rate in nozzle is calibrated by experiments, which will be reported in the result section (i.e., $\dot{\gamma} = 100 s^{-1}$).

3.4.2. Physical validation

To ensure printability of the designed material and confirm rheological measurement results, a physical test was performed. All the experimental samples containing different solvent concentrations were separately loaded into the syringes' barrel and pressure was applied to the syringes' plunger. Then, the material flow was observed to determine the composition which had the capability to form a continuous flow. Moreover, honeycomb structures were 3D printed to study material capability to keep its shape after being deposited on the surface.

4. Results and discussion

4.1. Interfacial interaction between fiber and matrix

The existence of modifications in the chemical bonding in the NaOH-treated, NaOH/silane-treated and untreated hemp fibers
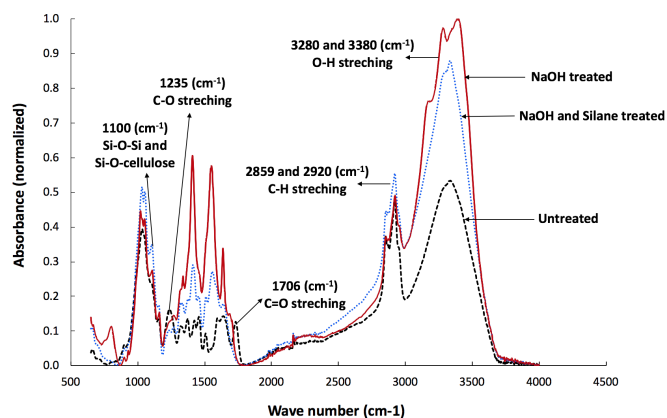
Figure 3: Fourier transform infrared (FT-IR) spectrum for treated and untreated hemp fibers.
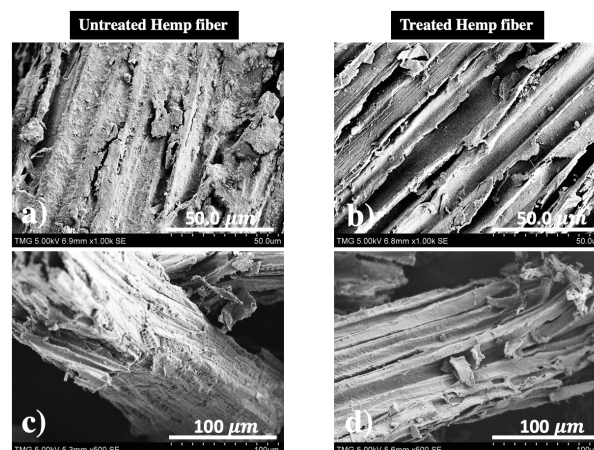

Figure 4: SEM images of (a,c) untreated and (b,d) NaOH-treated hemp fibers.

Figure 5: Fractured surfaces of HFRS with (top) untreated and (bottom) NaOH/silane-treated fibers.

were determined by FT-IR spectroscopy. Figure 3 demonstrates the spectra of treated and untreated hemp fibers. The peaks around 3280 and 3380cm^{-1} confirmed the presence of hydrogen bonded O-H stretching (the functional group of alcohols) in the fiber components. There is a significant increase in the absorption of this O-H region after NaOH treatment. This is due to the withdrawal of hemicellulose and lignin and thus increasing the number of exposed O-H groups from the surface of the fibers. The O-H group is the key in the interaction between fibers and silane coupling agent. The peak around 2859 and 2920cm^{-1} corresponds to C-H stretching vibration from aliphatic saturated compounds, like aliphatic moieties in cellulose and hemicellulose. The peak 1706cm^{-1} resulted from the vibrational stretching of carbonyl groups (C=O) is related to hemicelluloses and lignin. The intensity of this peak is decreased, and it illustrates the removal of lignin and hemicelluloses after NaOH treatment. Moreover, the peak intensity around 1235cm^{-1} ascribed C-O stretching of acetyl groups in the hemicellulose also diminished by the NaOH treatment. These results proved that the NaOH treatment can decrease the amount of non-cellulosic parts on the fibers surface leading to a better interaction between the two phases. The appearance of the peak around 1100cm^{-1} is corresponding to asymmetric stretching of Si-O-Si and Si-O-cellulose. The intensity of this peak increased after silane treatment, meaning that the silane coupling agent was grafted on the fiber surface. The polysiloxane has higher functional groups compared with fiber surface, which can easily react with the functional group of polymer matrix and established stable bonds. These adjustments are required for natural fibers used as reinforcement for polymer matrix.

4.2. Morphology of the hemp fibers

Figure 4 demonstrates the surface micrographs of untreated and NaOH-treated hemp fibers. SEM images show that the surface of untreated hemp fiber was relatively flat, leading to smaller surface area to bond with the polymer matrix. The NaOH treatment removed the noncellulosic parts like pectin, wax and lignin, and thus increased the roughness (Rz) of the fiber surface. This rougher surface facilitated the mechanical interlocking between fiber and silicone matrix. Therefore,

NaOH treatment increased the effective surface area available to contact with the matrix.

To investigate the interaction between fibers and matrix, scanning image analysis was performed on the fractured samples after tensile test to study the fiber distribution in the matrix and the adhesion between the two phases. Figure 5 represents SEM images of the impact fracture surface of the composites. The top of this figure illustrates that untreated fibers were presented in the form of fiber bundles instead of an uniform distribution. It is also demonstrated that there is poor adhesion between the untreated fiber and the matrix, evidenced by the pull-out holes in the matrix. There are even voids between both the components in the interfacial region.

Figure 5 (bottom) demonstrates the effect of NaOH and silane treatments on the interfacial interaction between the hemp fibers and the silicone matrix. It can be seen that fibers are totally covered by the matrix and there is no void between the two phases. In fact, the interfacial adhesion is affected by the changes of surface topography, because the higher the roughness of the fiber, the better mechanical interlocking between the fiber and the matrix. Therefore, the chemical treatments improved the adhesion at the interface leading to higher mechanical properties.
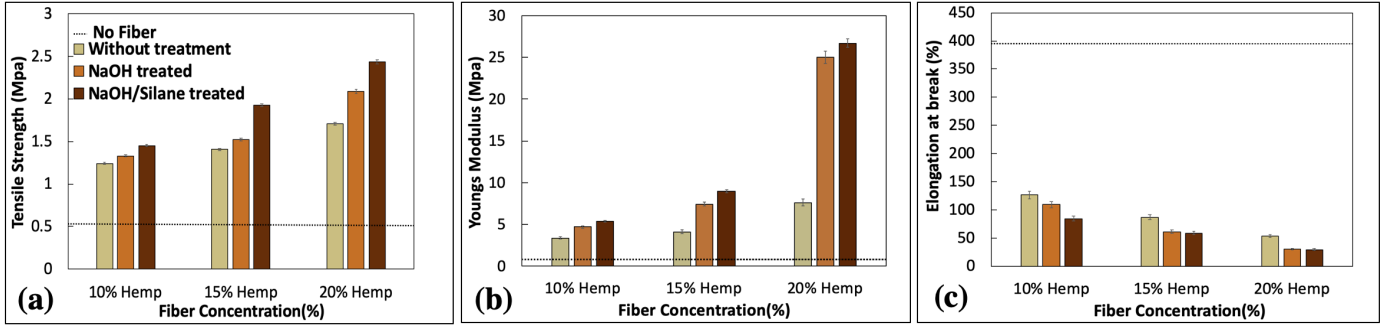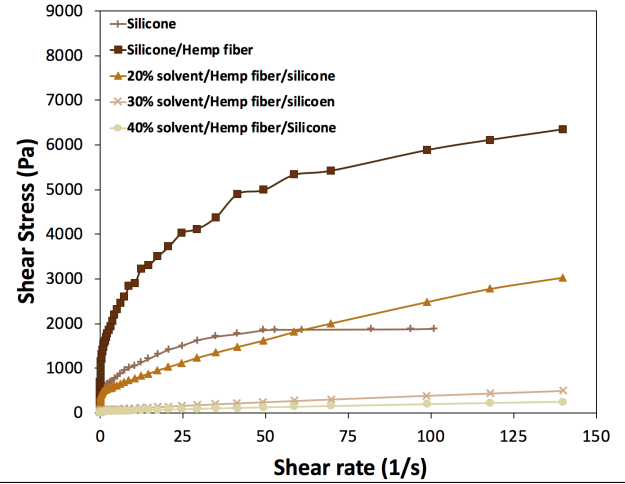
5

Figure 6: Mechanical properties of HFRS with different fiber concentrations; (a) Tensile strength,(b) Young's modulus, (c) Elongation at break.

4.3. Mechanical properties

Tensile strength and modulus for different compositions of untreated, NaOH-treated, and NaOH/silane-treated HFRS composites are presented in Figure 6. The samples here were fabricated by molding method to investigate impact of fiber loading on tensile strength and modulus. It is illustrated that with the increase of fiber content in the silicone matrix, the tensile strength and modulus were also increased. Compared with the pure silicone, the incorporation of 10%, 15%, and 20% of untreated hemp fibers increased tensile strength by 51%, 61%, and 68% and increased tensile modulus by 86%, 89%, and 94%, respectively. This can verify that the applied stress can be successfully distributed to the hemp fibers by the silicone matrix, and also proved that the silicone and the hemp fibers are compatible and they can form a composite material. Moreover, the results show that a higher fiber loading can tolerate a higher load before failure, meaning that the hemp fibers can act as a carrier of load and stress such that an uniform stress distribution is obtained [32, 33].

Comparing the fibers with and without treatments, the incorporation of 10%, 15%, and 20% of NaOH/silane-treated HFRS improved tensile strength by 14%, 27 %, and 29%, and tensile modulus by 37%, 54%, and 71%, respectively, compared with the untreated HFRS. As untreated fibers are covered by wax and contamination, there is a poor adhesion between hemp fiber and the silicone matrix. Consequently, the stress cannot be transferred effectively from matrix to fiber. In contrast, the significant increase in tensile strength of NaOH/silane-treated HFRS composites reflects that there is a better interfacial interaction between the fiber and the matrix. The improvement in fiber/matrix interaction is ascribed by the enriched roughness on the surface of the fibers and chemical bonding between functional groups of polysiloxane and functional groups of silicone. For the reader's reference, comparing with other reinforcements of silicone, Junhua et al. [34] showed that the incorporation of carbon nanotubes (CNT) in silicone improved tensile modulus by 60% and strength by 47%. Therefore, hemp fibers are not as strong as CNT, but their reinforcing performance are comparable. Moreover, hemp fibers are green and much lighter.

Figure 6 (c) shows the effect of fiber incorporation on elongation at break. As it was expected, the elongation at break of composites decreased by the incorporation of fibers. The higher the fiber content, the higher restriction for molecular motion
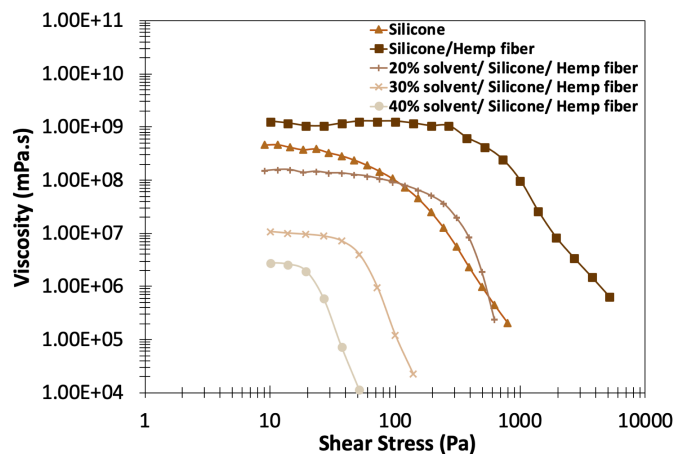

	k	n
Silicone	564.74	0.2842
Silicone/Hemp fiber	1526.2	0.2923
20 wt% solvent/Silicone/Hemp fiber	458.43	0.3126
30 wt% solvent/Silicone/Hemp fiber	51.351	0.3647
40 wt% solvent/Silicone/Hemp fiber	25.39	0.3872

Figure 7: Shear stress-shear rate results for all experimental samples.

and thus the lower ductility. The elongation at break reduced to only 44% for the HFRS with 20% NaOH/silane-treated hemp fiber. In other words, the incorporation of more than 15% hemp fibers in the silicone matrix showed a low ductility and presented a challenge in 3D printing as it increased silicone viscosity and changed its curing time. Therefore, 15% fiber loading was fixed as an upper limit, and all the following experiments were conducted with **15 wt% fibers**.

4.4. Shear rate in nozzle

Figure 7 shows the graph of shear stress against shear rate for various samples. Fitting the Power Law equation to each of the curve, the coefficients k and n in Eq.(2) can be obtained and they are listed in the table as well. These coefficients were employed to predict and analyze the condition as present in the nozzle using Eq.(1). The calculations revealed that the shear rate inside the nozzle is around $100 s^{-1}$ for all experimental samples.

6

	Yield stress (Pa)
Silicone	85.40
Silicone/Hemp fiber	440.76
20 wt% solvent/Silicone/Hemp fiber	152.64
30 wt% solvent/Silicone/Hemp fiber	45.79
40 wt% solvent/Silicone/Hemp fiber	21.82

Figure 8: Shear stress ramp for all experimental samples.

4.5. Yield stress measurements

Figure 8 demonstrates the viscosity – shear stress curves, which give information about yield stress. Yield stress was determined using the intersection of the plateau region (where the material is deformed elastically) and the region that the viscosity drops and the material starts to flow. The table in Figure 8 summarizes the results for different samples. The yield stress of the pure silicone is $85.4 Pa$. The samples with 30 wt% and 40 wt% solvent have lower yield stress values of 45.79 and $21.82 Pa$, respectively. This means that a lower force is needed to extrude the materials. However, having a yield stress only half of the printable silicone, the material probably cannot maintain its shape after printing. The composition containing 20 wt% solvent displayed a higher yield stress ($152.64 Pa$). This means that this material has a higher ability to keep its shape after extrusion.

The results also show that the pure HFRS (i.e., no solvent added) requires a much higher stress ($440.76 Pa$) compared to the other samples including the printable silicone. This demonstrated that the pure HFRS is too viscous and not printable. In the following experiments, although the data of pure HFRS are included for completeness, the discussion will mainly focus on finding a concentration of solvent for printability.

4.6. Shear thinning characterization

Figure 9 (a) demonstrates the shear viscosity profiles of all the samples against the range of share rate $[0.01\ 100]s^{-1}$, which were obtained by rheology measurements. All experimental samples displayed shear thinning behavior, in which the viscosity decreases over the increasing shear rate. The samples with 30 wt% and 40 wt% solvent demonstrate significantly lower viscosities compared to the pure silicone. The shear thinning profile for the sample with 20 wt% solvent aligned closely to

the pure silicone, which is printable. In other words, the composition of HFRS containing 20 wt% solvent has a similar shear thinning characteristics to the silicone, and it is more likely to be printable.

4.7. Recovery behaviour

Figure 9 (b) demonstrates the recovery behaviours for different solvent concentrations, using the time profile described in Sec. 3.4.1 (i.e., shear rate of $0.01 s^{-1}$ for first $200 s$, $100 s^{-1}$ for the next $100 s$, and $0.01 s^{-1}$ for the rest). Since a high shear rate in the middle decreased the viscosity of the samples, the recovery behaviour can be seen from how long it took for each sample to return its viscosity. The pure silicone has a rapid recovery ($50 s$) after exposing under a high shear rate. This shows that the pure silicone can quickly increase its viscosity after extrusion so that it can keep its printed shape and thus it is printable. It can be observed that it takes more than $140 s$ for the samples containing 30 wt% and 40 wt% solvent to get steady in viscosity. This is another evidence that samples with 30 wt% and 40 wt% solvent could cause difficulties in formation of continuous flow and shape fidelity, showing unprintability characteristics. In contrast, the composition containing 20 wt% solvent exhibits shorter recovery time to its initial viscosity (i.e., $< 75 s$). Therefore, the sample with 20 wt% solvent concentration exhibits closer printability characteristics to the pure silicone.

4.8. Extrusion stability

To confirm the rheological results, material flow was also monitored during extrusion. Figure 10 demonstrates the material flow for different samples with different compositions. The sample with 40 wt% solvent (Figure 10 (a)) demonstrated only droplet formation and could not form consistent material flow. The sample with 30 wt% solvent (Figure 10 (b)) displayed partial fiber formation, and the material flow was inconsistent and short. Therefore, both the samples with 30 and 40 wt% solvent exhibited unprintable behavior in line with the rheological results. In contrast, the sample with 20 wt% solvent (Figure 10 (c)) showed continuous and consistent material flow, which are the required characteristics for 3D printability.

In addition, hexagonal honeycomb structures were 3D printed to determine shape fidelity characteristics of different compositions. Figure 11 shows the 3D-printed hexagonal honeycomb structures with 40, 30, and 20 wt% solvent concentrations over curing process. The images clearly show that structures containing 40 and 30 wt% solvent concentrations did not keep the hexagon shape, but the one with 20 wt% solvent was able to maintain it. These observations are in agreement with the rheological results, and it is concluded that the composition with **20 wt% solvent** is suitable for 3D printing.

4.9. Dynamic properties of HFRS composites

Figure 12 illustrates the resistance to tensile stress and shear stress – storage modulus (G') and loss modulus (G"). The results showed an improvement in storage modulus over time for HFRS composite compared with pure silicone. This enhancement is due to the higher restriction executed by the fibers on
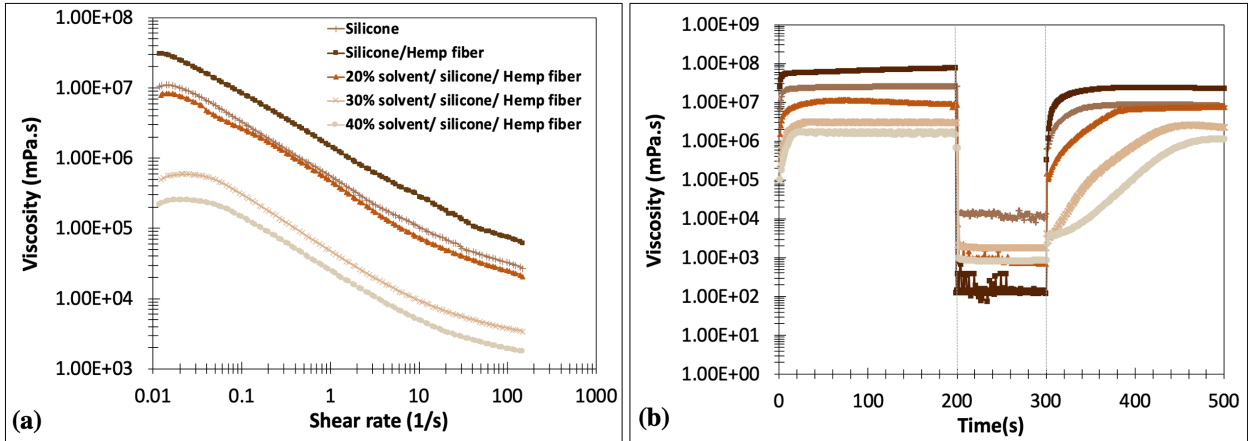
7

Figure 9: Rheological evaluation. (a) Shear-viscosity results for all experimental samples. (b) Recovery behavior of experimental samples to determine material behavior under a shear rate ($100 s^{-1}$) to near-zero shear to simulate the environment experienced by the materials during extrusion printing.
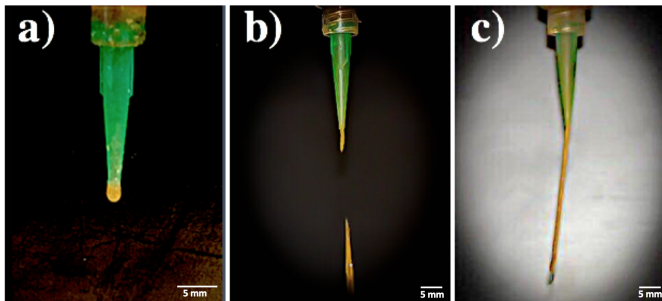

Figure 10: Effect of solvent concentration on material flow; a) 40 wt%, b) 30 wt%, and c) 20 wt% solvent.
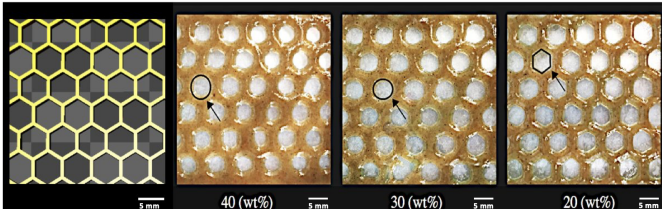

Figure 11: Effect of solvent concentration on 3D printing shape fidelity.

Figure 12: The effect of hemp fibers on shear storage modulus of silicone.

the matrix, which increased the stress transfer at the fiber interface. As expected, the pure silicone behavior was dominated by loss modulus until the gel point which is the point where it converted from viscous fluid structure to elastic structure. The behavior of HFRS composites was dominated by the storage modulus throughout the entire curing time. Due to the incorporation of fillers, the composite demonstrates solid-like behavior. This elastic characteristic of the material is confirming the material capability to maintain its shape until it is cured over time.

4.10. Mechanical property of 3D-printed HFRS

To compare the mechanical properties of the molded and 3D-printed samples, dog bone shape samples were produced. For 3D printing, the toolpaths are aligned at 0° angle as shown in Figure 13. Figure 14 shows the tensile strength and Young's modulus of molded and 3D-printed HFRS composites. It is evident that the 3D-printed samples have higher stiffness and tensile strength in comparison with the molded counterparts. The
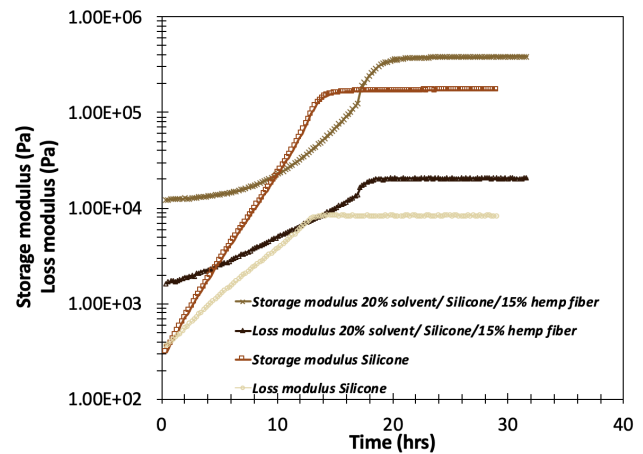
enhanced mechanical properties could be explained by the fact that hemp fibers were aligned during 3D printing process. SEM images in Fig. 15(b,c) show the directional alignment of hemp fibers along printing direction. In contrast, for the molded samples, there is no fiber alignment as shown in Fig. 15(a). After mixing the fibers with the matrix, the fibers are aligned randomly in the solution. Direct ink writing (DIW) is an extrusion-based 3D printing. When the material reach the nozzle tip, the fibers are aligned under the shear and extensional flow field that applied by nozzle during 3D printing. In fact, under the simple shear flow fibers tend to align in the shear direction. This is leading to higher mechanical properties compare to those fabricated by mold, which aligned with the findings of other works reporting the impact of fiber direction on mechanical properties [35, 36]. In addition, there is a densification of the paste when the material is extruded through the nozzle. Figure 16 shows the fractured surface of the 3D-printed and molded samples after tensile test. SEM images demonstrate that the extent of void inclusion in molded samples. Indeed, there are large voids within the molded samples compared to the 3D-printed samples with the same composition. It shows that the bubbles were removed as the material passed through the nozzle.
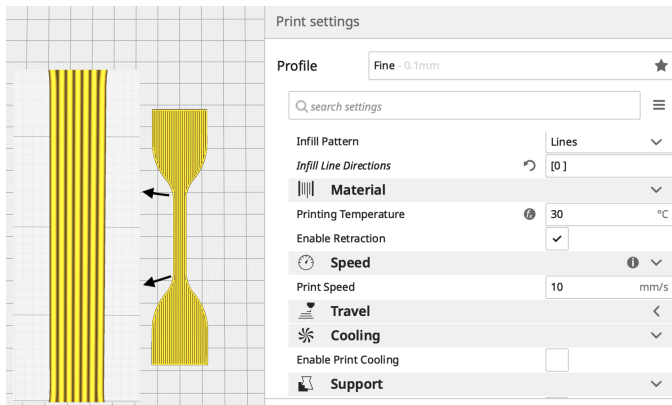
8

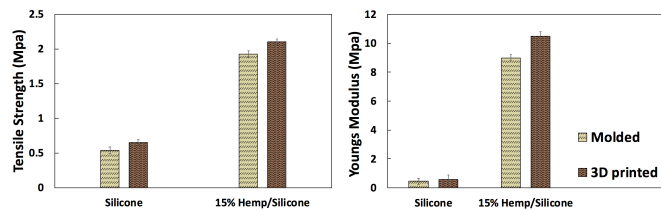Figure 13: Toolpath and setting for 3D printing the dog bone shape.

Figure 14: Mechanical properties of 3D printed samples.

Therefore, the 3D-printed part has a denser structure leading to improved mechanical properties. Note that the material was already evacuated before solidification, since the fibers were distributed in the silicone matrix using a vacuum mixer (see Sec. 2.3).

A simple soft gripper using HFRS is 3D-printed and it was compared with its silicone counterparts (Figure 17). To make a comparison between the strength of the two grippers, a micro force sensor was used (Figure 18). The soft grippers were held on a flat plate, and an adjustable angle clamp was used to provide the same configuration for each soft gripper. It can be seen that there is a significant difference in the measured voltage between the silicone gripper and the HFRS gripper (i.e., $215V$ vs. $586V$). After calibration, it means that the HFRS gripper is capable of lifting around $130g$, but the silicone gripper can only lift around $30g$. Therefore, the incorporation of hemp fibers significantly enhanced the silicone properties and made it stronger.

5. Conclusions

This study presented the design of a new 3D-printable elastomeric composites, developed by the incorporation of hemp fiber in silicone – hemp fiber reinforced silicone (HFRS), with enhanced mechanical properties. One of the main challenges is the poor compatibility between the fibers and matrix. Therefore, alkali and silane treatments were used to modify the surface of hemp fibers. Alkali and silane treatments improved tensile strength and modulus of the HFRS composites by 27% and 54%, respectively, compared to the one with untreated hemp fibers. Alkali treatment increased the surface roughness of the hemp fiber and exposed more reactive O-H groups on the fiber surface to facilitate chemical bonding. Moreover, silane cou-

pling agent acts as a bridge between hemp fiber and silicon. Therefore, silane treatment increased the fiber-matrix interfacial bonding strength resulted in enhanced mechanical properties.

To enhance the mechanical properties of the HFRS composites and to ensure its printability, we need to determine a suitable mixing composition. Therefore, mechanical tests and microscopic examinations were used to figure out the hemp fibers loading that can provide desirable mechanical properties. It was found that incorporation of 15 wt% fiber increased tensile strength and modulus of HFRS composites by 61% and 89%, respectively, compared to silicone.

The challenge with 3D printing this material was that the high viscosity after mixing with fibers made it unprintable. Different solvent concentrations were added to the composition to determine the composition with printable behavior. Rheological evaluation and physical validation were performed to obtain printable material. The results revealed that the HFRS with 15wt% hemp fibers and 20 wt% solvent exhibited 3D-printable behavior. This composition was capable to form continuous flow and keep its shape after deposition. Mechanical testing demonstrated that 3D printed products have improved mechanical properties compared to the molded samples.

The main goal in this study is to examine the printability of HFRS, but other performances were not reported. In the future, we will have a complete report on different mechanical properties of the developed material, and we will also study how the printing orientation and toolpath affect the mechanical properties of HFRS.

References

[1] R. Matsuzaki, M. Ueda, M. Namiki, T. K. Jeong, H. Asahara, K. Horiguchi, T. Nakamura, A. Todoroki, Y. Hirano, Three-dimensional printing of continuous-fiber composites by in-nozzle impregnation, Scientific reports 6 (2016) 23058.

[2] Y. Tao, H. Wang, Z. Li, P. Li, S. Shi, Development and application of wood flour-filled polylactic acid composite filament for 3d printing, Materials 10 (2017) 339.

[3] A. L. Duigou, M. Castro, R. Bevan, N. Martin, 3d printing of wood fibre biocomposites: From mechanical to actuation functionality, Materials & Design 96 (2016) 106–114.

[4] X. Wang, M. Jiang, Z. Zhou, J. Gou, D. Hui, 3d printing of polymer matrix composites: A review and prospective, Composites Part B: Engineering 110 (2017) 442 – 458.

[5] J. J. Martin, E. F. Brad, M. E. Randall, Designing bioinspired composite reinforcement architectures via 3d magnetic printing., Nature communications (2015) 1–7.

[6] Y. Yang, Z. Chen, Z. Z. X. Song, J. Zhang, K. K. Shung, Q. Zhou, Biomimetic anisotropic reinforcement architectures by electrically assisted nanocomposite 3d printing., Advanced materials (2017) 1605750.

[7] P. Song, Z. J. Peng, Y. L. Yue, H. Zhang, Z. Zhang, Y. C. Fan, Mechanical properties of silicone composites reinforced with micron-and nano-sized magnetic particles., Express Polymer Letters 7 (2013).
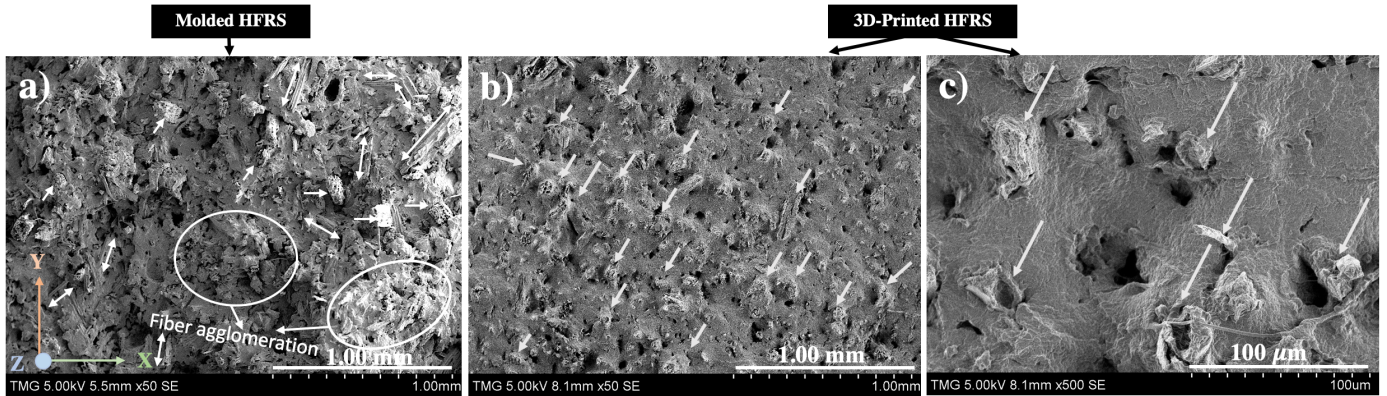
Figure 15: a) Cross-section of molded HFRS, where fibers are distributed randomly; b,c) Cross-section of 3D-printed samples, where hemp fibers were aligned along the 3D printing direction (z).
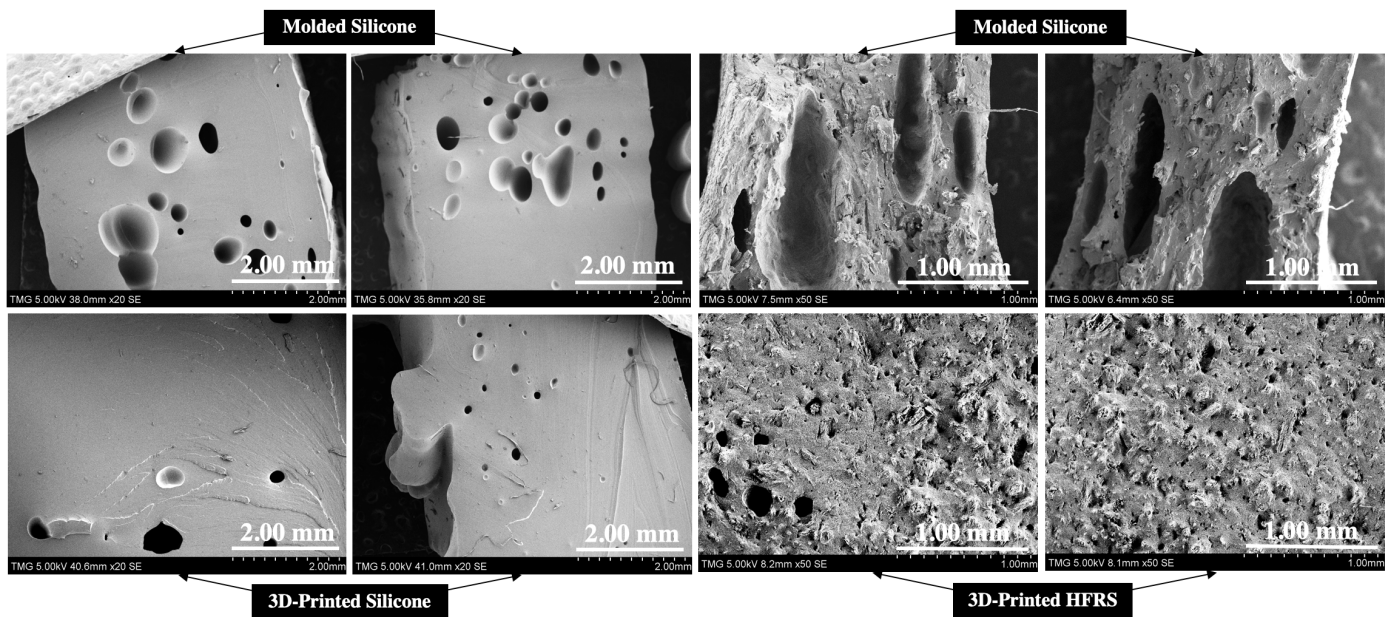

Figure 16: Cross-sections of molded and 3D-printed samples.

Figure 17: A soft gripper fabricated by (left) pure silicone and (b) HFRS using the DIW 3D printing method.

[8] A. K. Bledzki, V. E. Sperber, O. Faruk, Natural and wood fibre reinforcement in polymers, volume 13, iSmithers Rapra Publishing, 2002.

[9] R. Quarshie, J. Carruthers, Technology overview biocomposites, sec. 7.11, 2014. Https://netcomposites.com/media/1211/biocomposites-guide.pdf.

[10] G. Momen, M. Farzaneh, Survey of micro/nano filler use to improve silicone rubber for outdoor insulators, Rev. Adv. Mater. Sci 27 (2011) 1–13.

[11] M. Thiruchitrambalam, A. Athijayamani, s. Sathiyamurthy, A. Thaheer, A review on the natural fiber-reinforced polymer composites for the development of roselle fiber-reinforced polyester composite, Journal of Natural Fibers 7 (2010) 307–323.

[12] A. L. Duigou, M. Castro, R. Bevan, N. Martin, 3d printing of wood fibre biocomposites: From mechanical to actuation functionality, Materials and Design 96 (2016) 106 – 114.

[13] W. Xu, . Pranovich, P. Uppstu, X. Wang, D. Kronlund, J. Hemming, Novel biorenewable composite of wood polysaccharide and polylactic acid for three dimensional printing, Carbohydrate Polymers 187 (2018) 51 – 58.

[14] A. B. Asha, A. Benozir, A. Sharif, M. E. Hoque, Interface interaction of jute fiber reinforced pla biocomposites for potential applications, in: Green Biocomposites, Springer, 2017, pp. 285–307.

[15] M. Brahmakumar, C. Pavithran, R. Pillai, Coconut fibre reinforced polyethylene composites: effect of natural waxy surface layer of the fibre on fibre/matrix interfacial bonding and strength of composites, Composites Science and Technology 65 (2005) 563 – 569. JNC13-AMAC-Strasbourg.

[16] Karthikeyan, Rajasekaran, Analysis of Natural Fiber Orientation in Polymer Composites Produced by Injection Molding Process, Ph.D. thesis, University of Toronto (Canada), 2017.
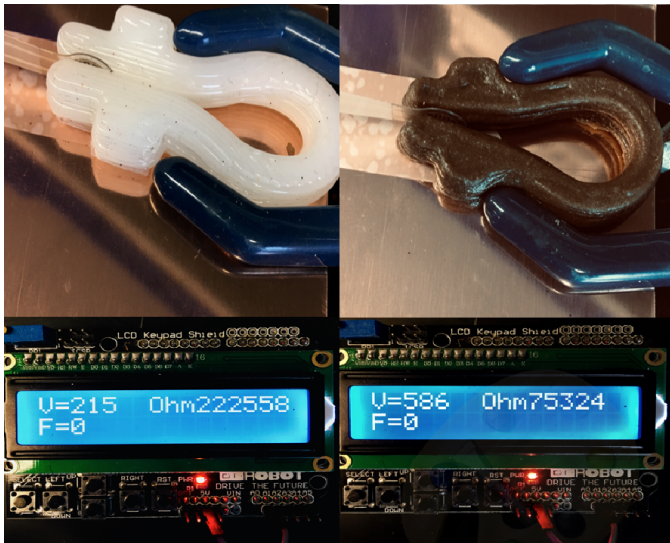
Figure 18: Using micro force sensor to measure the applied forces.

[17] J. Rossiter, P. Walters, B. Stoimenov, Printing 3d dielectric elastomer actuators for soft robotics, in: Electroactive Polymer Actuators and Devices (EAPAD) 2009, volume 7287, International Society for Optics and Photonics, 2009, p. 72870H.

[18] Ontario hemp materials, 2017. Https://www.ontariohemp.ca/.

[19] S. Kalia, B. S. Kaith, I. Kaur, Pretreatments of natural fibers and their application as reinforcing material in polymer composites—a review, Polymer Engineering & Science 49 (2009) 1253–1272.

[20] S. Theresa, P. Selvum, K. Alastair, N. Haibin, Hemp fiber reinforced polypropylene composites: The effects of material treatments, Composites Part B: Engineering 114 (2017) 15 – 22.

[21] M. S. Huda, L. T. Drzal, A. K. Mohanty, M. Misra, Effect of fiber surface-treatments on the properties of laminated biocomposites from poly(lactic acid) (pla) and kenaf fibers, Composites Science and Technology 68 (2008) 424 – 432.

[22] M. Abdelmouleh, S. Boufi, M. N. Belgacem, A. Dufresne, Short natural-fibre reinforced polyethylene and natural rubber composites: Effect of silane coupling agents and fibres loading, Composites Science and Technology 67 (2007) 1627 – 1639.

[23] E. T. N. Bisanda, M. P. Ansell, The effect of silane treatment on the mechanical and physical properties of sisal-epoxy composites, Composites Science and Technology 41 (1991) 165 – 178.

[24] M. Huda, L. T. Drzal, A. K. Mohanty, M. Misra, Effect of chemical modifications of the pineapple leaf fiber surfaces on the interfacial and mechanical properties of laminated biocomposites, Composite Interfaces 15 (2008) 169–191.

[25] F. Tavassoli, M. Razzaghi, B. Mohebby, Hydrothermally treated wood as reinforcing filler for natural rubber bio-composites, Journal of Polymer Research 25 (2018) 3.

[26] S. D. printing, Ultimaker and the discov3ry paste extruder, 2018. Https://www.structur3d.io/discov3ry-complete/.

[27] Structured printing, 2016. Https://www.structur3d.io/.

[28] Ultimaker and the discov3ry paste extruder, 2016. Https://www.structur3d.io/discov3ry-complete/.

[29] R. Suntornnond, E. Y. Tan, J. An, C. K. Chua, A mathematical model on the resolution of extrusion bioprinting for the development of new bioinks, Materials 9 (2016) 756.

[30] Q. H. Nguyen, N. D. Nguyen, Incompressible non-newtonian fluid flows, in: Continuum Mechanics-Progress in fundamentals and Engineering applications, InTech, 2012.

[31] M. Panalitical, Using the power law model to quantify shear thinning behavior on a rotational rheometer, 2015. Https://www.azom.com/article.aspx?ArticleID=11624.

[32] K. Senthilkumar, N. Rajini, N. Saba, M. Chandrasekar, M. Jawaid, S. Siengchin, Effect of alkali treatment on mechanical and morphological properties of pineapple leaf fibre/polyester composites, Journal of Polymers and the Environment 27 (2019) 1191–1201.

[33] M. R. Sanjay, P. Madhu, M. Jawaid, P. Senthamaraikannan, S. Senthil, S. Pradeep, Characterization and properties of natural fiber polymer composites: A comprehensive review, Journal of Cleaner Production 172 (2018) 566–581.

[34] J. Kong, Y. Tong, J. Sun, W. T. Y. Wei, C. C. Jayven, Electrically conductive pdms-grafted cnts-reinforced silicone elastomer, Composites Science and Technology 159 (2018) 208–15.

[35] H. A. Pierson, E. Celik, A. Abbott, H. De Jarnette, L. Sierra Gutierrez, K. Johnson, H. Koerner, J. W. Baur, Mechanical properties of printed epoxy-carbon fiber composites, Experimental Mechanics 59 (2019) 843 – 857.

[36] N. Kumar, P. Avinash, A. Singh, K. Debnath, Effect of fiber orientation on the tensile and wear properties of flax fiber-reinforced composites, in: B. B. Biswal, B. K. Sarkar, P. Mahanta (Eds.), Advances in Mechanical Engineering, Springer Singapore, Singapore, 2020, pp. 505–513.